Supplementary Material

to

Attributing the US Southwest's recent shift into drier conditions

Flavio Lehner[1*], Clara Deser[1], Isla R. Simpson[1], Laurent Terray[2]

[1]Climate and Global Dynamics Laboratory, National Center for Atmospheric Research, Boulder, USA

[2]Climate, Environment, Coupling and Uncertainties group, Université de Toulouse, CERFACS/CNRS, Toulouse, France

[*] flehner@ucar.edu

Content

Table S1: List of model simulations used in this study. Historical, rcp45, and rcp85 refer to the CMIP5 radiative forcing protocols (Meinshausen et al. 2011). ERSSTv3b and ERSSTv4 refer to the Extended Reconstructed Sea Surface Temperature version 3b (Smith et al. 2008) and 4 (Huang et al. 2015). HadISST refers to the adley Centre Sea Ice and Sea Surface Temperature data set (Rayner et al. 2003). More details on the simulations can be found in the respective references. CESM website refers to http://www.cesm.ucar.edu/experiments/cesm1.1/LE.

Model family	Experimental setup	Forcing details	Time period	Ensemble members or number of models	Reference
CESM	Coupled CESM1-CAM5	historical, rcp85	1920-2100	40	(Kay et al. 2015)
CESM	TOGA CAM5	ERSSTv4, HadISST	1880-2014	10	CESM website
CESM	GOGA CAM5	ERSSTv4, HadISST	1880-2015	10	CESM website
CESM	Coupled CESM1-CAM5	Preindustrial control	2,200 years	1	(Kay et al. 2015)
CESM	Atmosphere-only CAM5	Climatological SSTs from CESM preindustrial control	2,600 years	1	CESM website
GFDL	Coupled CM2.1-AM2.1	historical, rcp45	1861-2015	10	(Kosaka and Xie 2016)
GFDL	GOGA AM2.1	ERSSTv3b, HadISST	1950-2012	10	(Kosaka and Xie 2016)
CMIP5	Coupled	historical, rcp85	1871-2099	40	various

Table S2: 1983-2012 trends over the US Southwest (region marked in Fig. 1a) for unadjusted and dynamically adjusted observed precipitation (GPCC) and surface air temperature (BEST). Uncertainty for unadjusted observations is based on the minimum and maximum trend in Newman et al. (2015) and given in square brackets. For dynamically adjusted trends, the result from EEMD/EEMD detrending is given, while the uncertainty is based all the different detrending methods tested (see section S1) and given in square brackets.

		Water year	**Oct-Dec**	**Jan-Mar**	**Apr-Jun**	**Jul-Sep**
Precipitation (%/30 yrs)	*Unadj.*	-19.3 [-21.4, -12.0]	-19.0 [-26.2, -9.2]	-26.7 [-29.7, -15.9]	-9.1 [-14.0, 1.5]	-29.3 [-36.6, -19.3]
	Dyn. adj.	-6.13 [-6.13, -0.8]	-3.4 [-9.6, -2.0]	-0.8 [-0.8, 11.9]	1.3 [1.3, 15.2]	6.2 [-5.1, 6.2]
Temperature (°C/30 yrs)	*Unadj.*	0.84 [0.68, 0.85]	1.01 [0.76, 1.08]	0.38 [0.28, 0.64]	0.46 [0.37, 0.56]	1.32 [1.09, 1.44]
	Dyn. adj.	0.49 [0.35, 0.79]	0.31 [-0.07, 0.61]	0.34 [0.34, 1.01]	0.50 [0.50, 0.89]	0.28 [0.28, 0.88]

S1. Detrending method prior to dynamical adjustment

For dynamical adjustment with constructed circulation analogues (CCA), a large number of analogues are required. Ideally, these analogues are not systematically skewed in their distribution of climate states they represent. In context of surface air temperature (SAT) it can be problematic to use CCAs from a climate significantly warmer or colder than the climate that one is trying to reconstruct, since an analogue from a warmer climate will falsely give the impression that a particular circulation pattern induced warmer conditions, when in the respective climate that particular circulation pattern might not have a tendency to induce warmer conditions (Smoliak et al. 2015). Note that this issue can also be exploited to study the changing influence of particular circulation patterns under transient climate conditions (Cattiaux et al. 2012). When using climate models, the issue can be avoided for example by creating CCAs from control simulations, which represent stationary climate states. For observations this is not possible, which is why an estimate of the climate non-stationarity, i.e., the forced anthropogenic trend, has to be removed before the observations can be used to create an un-skewed distribution of CCAs.

Different approaches to detrend SAT have been tested in Deser et al. (2016). Here we test whether and how precipitation (P) and sea level pressure (SLP) should be detrended before constructing the CCAs, since it is less clear *a priori* whether to detrend or not, due to a less robust understanding of the anthropogenically forced trend in these two variables compared to SAT (Gillett and Stott 2009; Hegerl et al. 2015). The following detrending methods are tested: (i) no detrending, (ii) removing the CESM LE mean, (iii) removing the CMIP5 multi-model mean across 40 models, and (iv) removing the first intrinsic mode function of the ensemble empirical mode decomposition (EEMD; Wu and Huang 2009). EEMD has the benefit of being non-parametric and is suited to deal with non-stationary and non-linear time-space phenomena; however, it is purely statistical. The CESM LE mean and CMIP5 multi-model mean have the benefit of being informed by physics; however, they include possible model biases. We apply these detrending methods in different combinations to P and SLP observations over the period 1901-2015 and investigate their impact on the 1983-2012 dynamically adjusted P and SLP trend over Western North America, i.e., same domain and time period as in the main paper (Fig. S1). While it is clear that the different methods yield slightly different results, they ultimately all reduce the drying trend over the US Southwest. The range of area-averaged P trends resulting from the different detrending methods is given in Table S2 and is comparable to the uncertainties in the unadjusted observations themselves. We thus conclude that it does not matter critically for the study here which detrending method is chosen. Maybe more interestingly, this also suggests that any forced gradual changes in SLP (if they exist in reality), do not notably affect our estimate of the general SLP influence on the observed P and SAT trends. For consistency, in the main paper we focus on the results from the detrending of SAT, P, and SLP with EEMD.

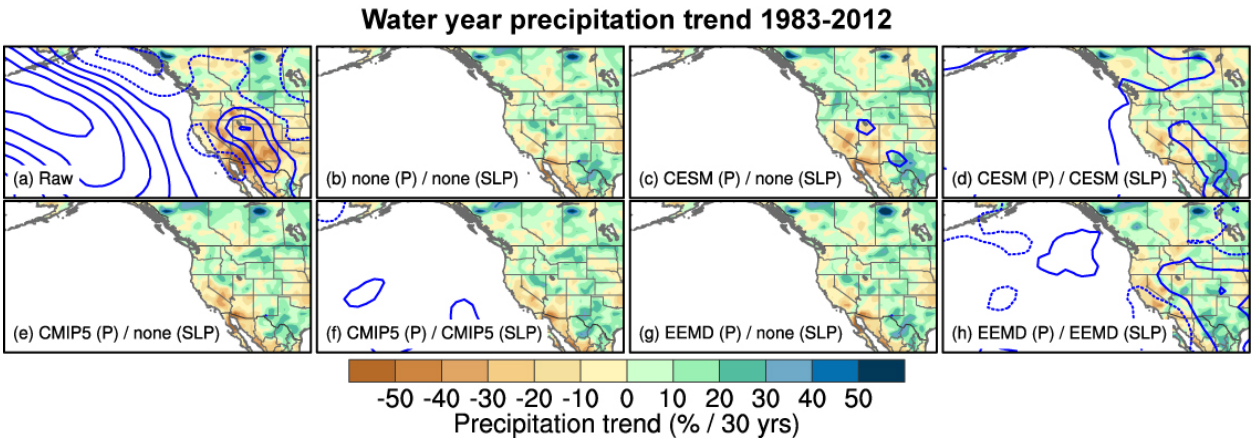

Figure S1: Water year precipitation (P), surface air temperature (SAT), and sea level pressure (SLP) trend from 1983 to 2012 from (a) observations (GPCC and TCR version 2c) and (b-h) after dynamical adjustment. Prior to dynamical adjustment, P, SAT, and SLP have been detrended with the methods indicated in the individual panels.

We dynamically adjust ensemble member #8 of the CESM LE, since it happens to show a similar shift from positive to negative PDO during 1983-2012 as observed (not shown) as well as a similar drying trend over the US SW. The dynamical adjustment of this simulation (and all other 39 CESM LE members, used in Fig. S4) is conducted in a similar fashion as for observations (Section 2.2). That is, 95 model years of CESM LE member #8 are used (1920-2015), 80 of which are selected randomly to form the CCAs, and the procedure is repeated 100 times. Instead of EEMD, we use the CESM LE 40-member mean (a good estimate of the model's forced response; Deser et al. 2016) to detrend precipitation, SAT, and SLP prior to dynamical adjustment.

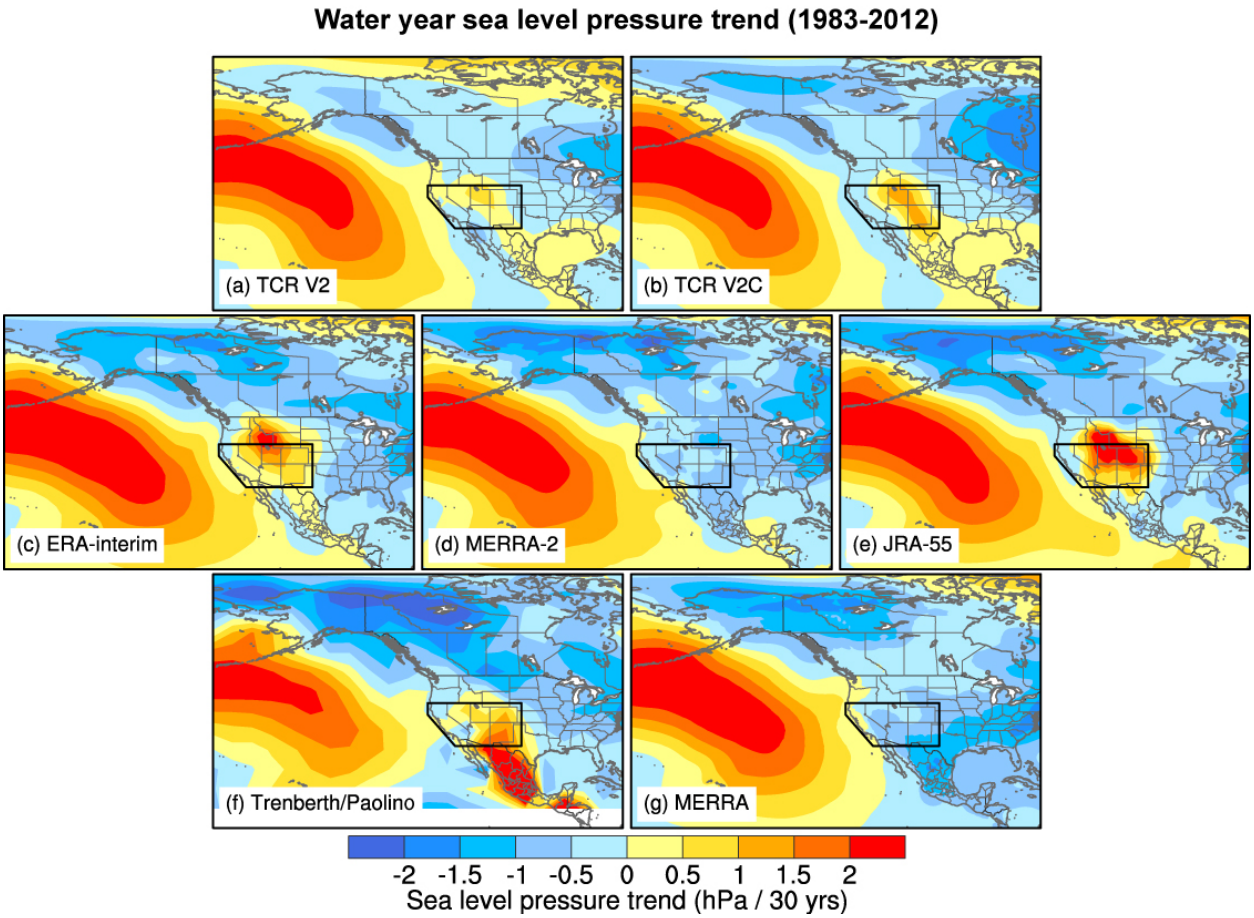

Figure S2: Water year sea level pressure (SLP) trend from 1983 to 2012 from different reanalysis datasets. While the positive SLP trend in the Aleutian Low is robust across datasets, the anomaly over the Western US varies across datasets in terms of location, magnitude, and sign. Similar results are seen in surface pressure (not shown).

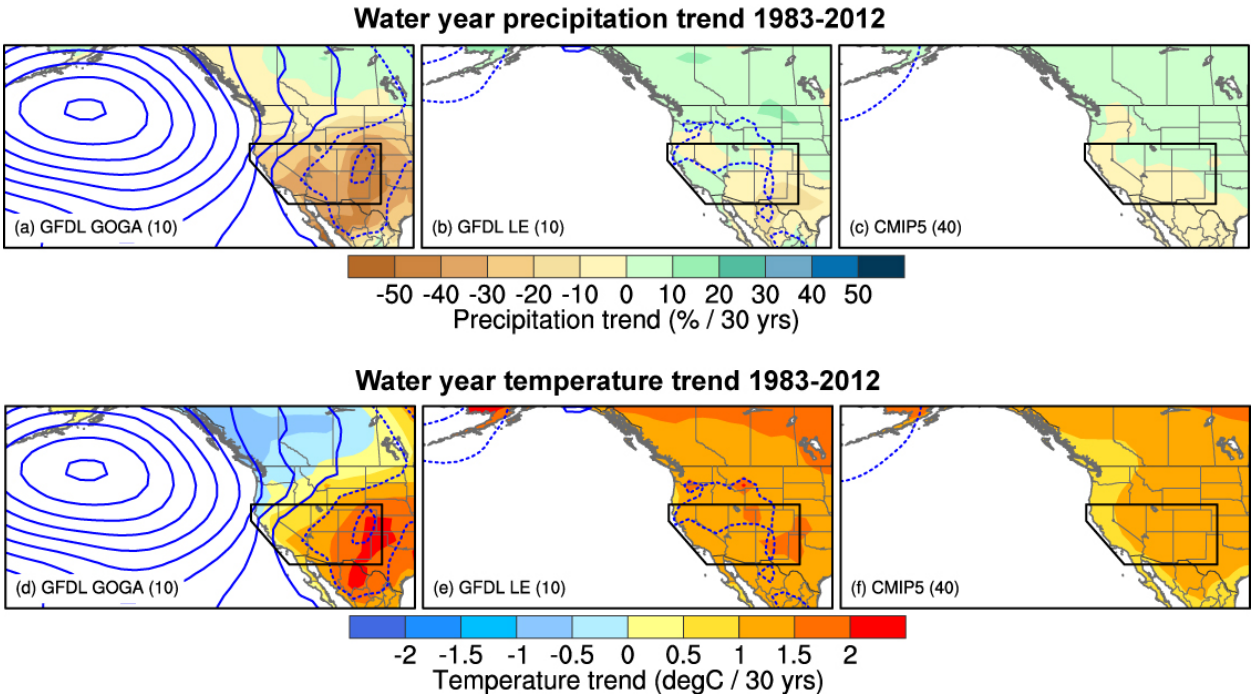

Figure S3: Water year precipitation and sea level pressure (SLP) trend from 1983 to 2012 from (a) GFDL GOGA, (b) GFDL LE, (c) CMIP5. (d-f) same as (a-c), but for surface air temperature and SLP. Number of simulations of each ensemble is given in brackets. Contours are sea level pressure trend in 0.5hPa 30 years^{-1} increments starting at ±0.25hPa.

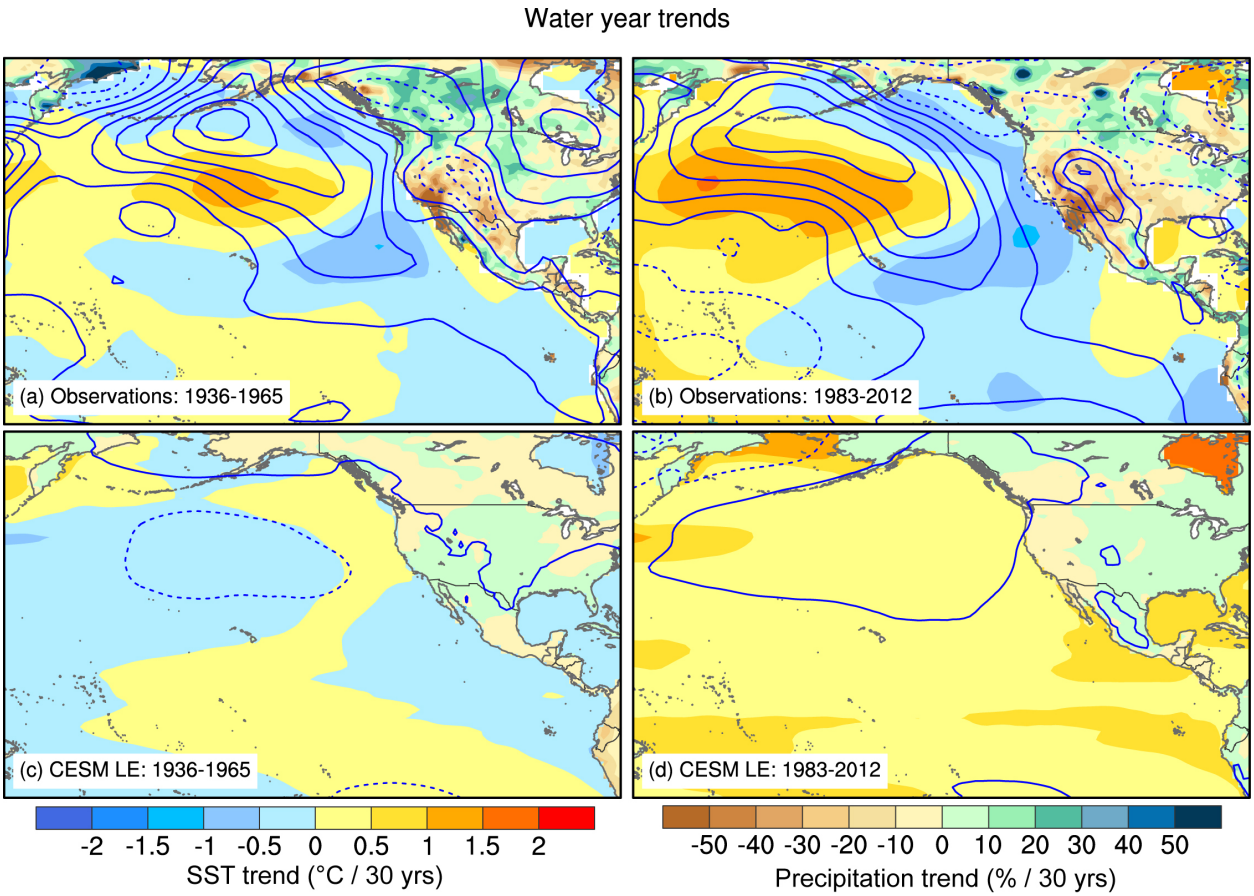

Figure S4: Water year sea surface temperature (SST), precipitation, and sea level pressure (SLP) trends for (a) observations 1936-1965, (b) observations 1983-2012, (c) ensemble mean of CESM LE 1936-1965, (d) ensemble mean of CESM LE 1983-2012. Contours are sea level pressure trend in 0.5hPa 30 years^{-1} increments starting at ±0.25hPa.

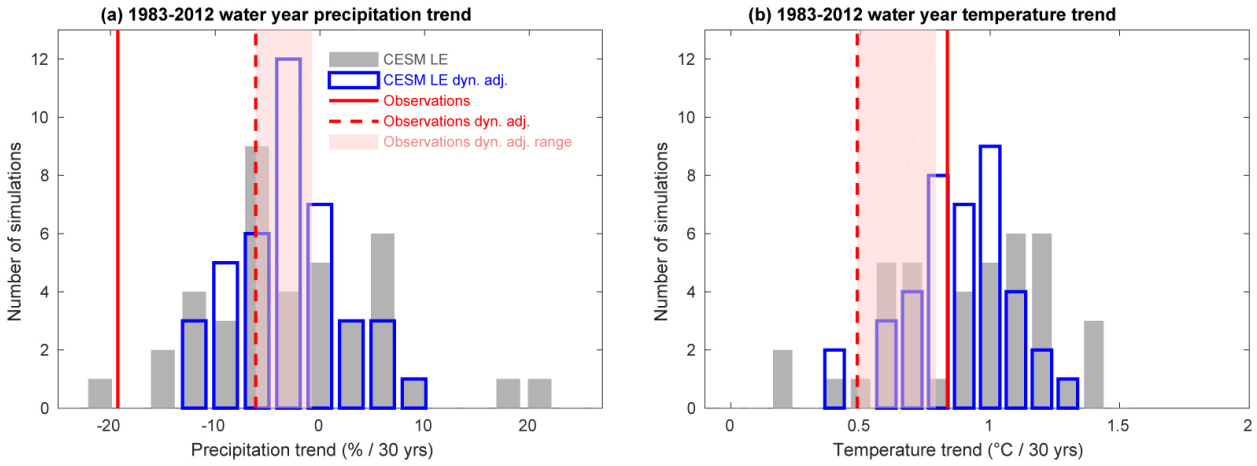

Figure S5: 1983-2012 water year trend averaged over the US Southwest for (a) precipitation and (b) surface air temperature from unadjusted and dynamically adjusted observations and all 40 CESM LE members. The uncertainty range for the dynamically adjusted observations (red shading) is based on the 7 different detrending approaches discussed in Section S1. The red dashed line marks the detrending approach used in the main text (EEMD/EEMD).

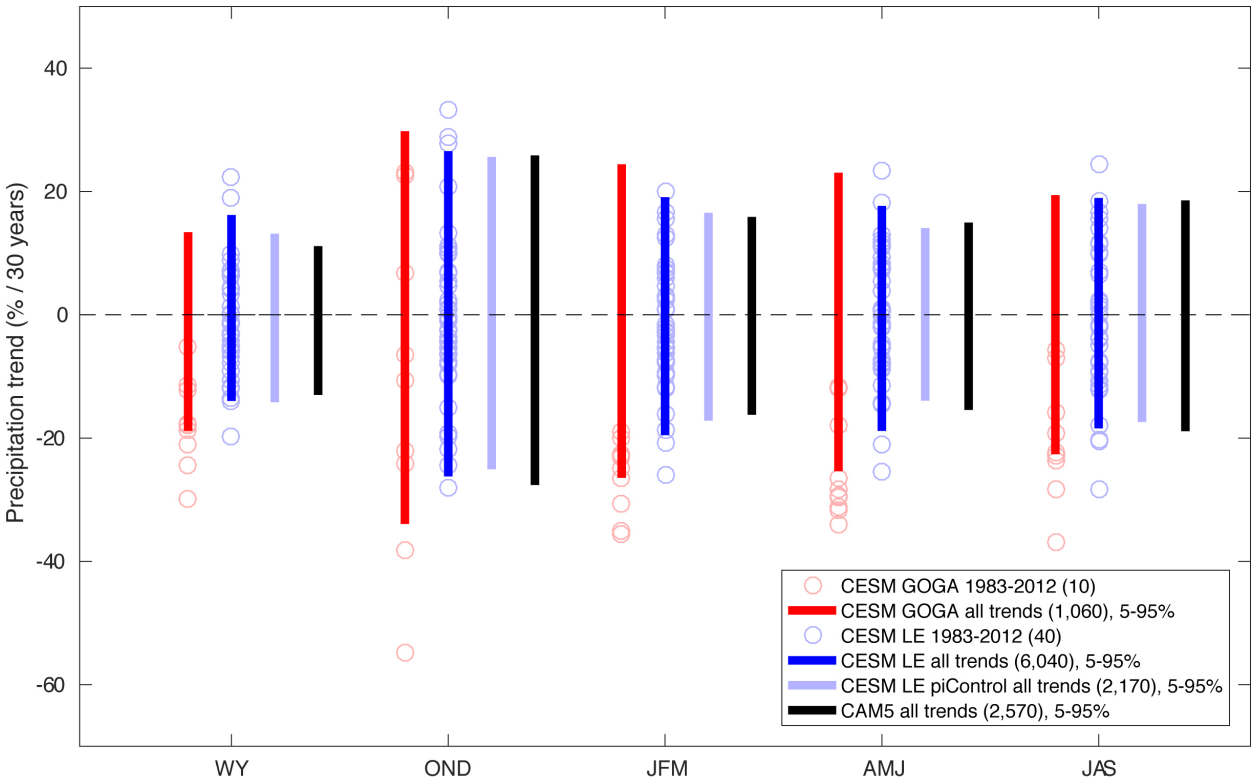

Figure S6: 30-year precipitation trends over the US SW from (red) CESM GOGA, (blue) CESM LE, (light blue) a 2,200-year long CESM preindustrial control simulation, and (black) a 2,600-year long atmosphere-only simulation with CAM5, the atmospheric component of CESM, in which climatological SSTs from the CESM preindustrial control simulation are prescribed perpetually. For the specific period 1983-2012, the individual simulations from CESM GOGA and CESM LE are shown with circles; all the other trends are summarized with vertical bars that represent the 5-95% range of the trend distribution. The seasons are marked on the x-axis as water year (WY), Oct-Dec (OND), Jan-Mar (JFM), Apr-Jun (AMJ), and Jul-Sep (JAS).

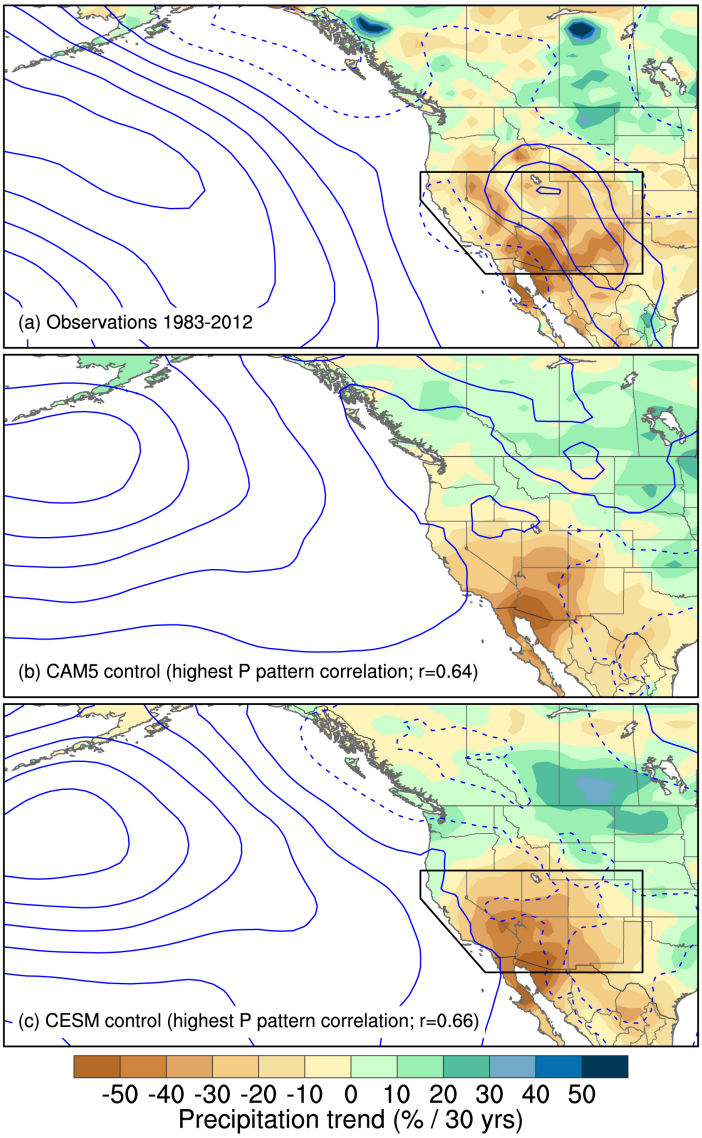

Figure S7: 30-year water year precipitation and sea level pressure trends from (a) observations, (b) CESM atmosphere-only control simulation with CAM5, and (c) CESM coupled preindustrial control simulation. For observations, the 1983-2012 trend is shown. For the two model simulations, the 30-year trend period with the highest precipitation pattern correlation with the observed trend pattern (over the entire domain of the Figure) is shown. Model trends are expressed relative to their long-term mean.

References

Cattiaux, J., P. Yiou, and R. Vautard, 2012: Dynamics of future seasonal temperature trends and extremes in Europe: A multi-model analysis from CMIP3. *Clim. Dyn.*, **38**, 1949–1964, doi:10.1007/s00382-011-1211-1.

Deser, C., L. Terray, and A. S. Phillips, 2016: Forced and internal components of winter air temperature trends over North America during the past 50 years: Mechanisms and implications. *J. Clim.*, **29**, 2237–2258, doi:10.1175/JCLI-D-15-0304.1.

Gillett, N. P., and P. a. Stott, 2009: Attribution of anthropogenic influence on seasonal sea level pressure. *Geophys. Res. Lett.*, **36**, L23709, doi:10.1029/2009GL041269.

Hegerl, G. C., and Coauthors, 2015: Challenges in quantifying changes in the global water cycle. *Bull. Am. Meteorol. Soc.*, **96**, 1097–1115, doi:10.1175/BAMS-D-13-00212.1.

Huang, B., and Coauthors, 2015: Extended reconstructed sea surface temperature version 4 (ERSST.v4). Part I: Upgrades and intercomparisons. *J. Clim.*, **28**, 911–930, doi:10.1175/JCLI-D-14-00006.1.

Kay, J. E., and Coauthors, 2015: The community earth system model (CESM) large ensemble project : A community resource for studying climate change in the presence of internal climate variability. *Bull. Am. Meteorol. Soc.*, **96**, 1333–1349, doi:10.1175/BAMS-D-13-00255.1.

Kosaka, Y., and S.-P. Xie, 2016: The tropical Pacific as a key pacemaker of the variable rates of global warming. *Nat. Geosci.*, **9**, 669–673, doi:10.1038/ngeo2770.

Meinshausen, M., and Coauthors, 2011: The RCP greenhouse gas concentrations and their extensions from 1765 to 2300. *Clim. Change*, **109**, 213–241, doi:10.1007/s10584-011-0156-z.

Newman, A. J., and Coauthors, 2015: Gridded Ensemble Precipitation and Temperature Estimates for the Contiguous United States. *J. Hydrometeorol.*, **16**, 2481–2500, doi:10.1175/JHM-D-15-0026.1.

Rayner, N. A., D. E. Parker, E. B. Horton, C. K. Folland, L. V. Alexander, D. P. Rowell, E. C. Kent, and A. Kaplan, 2003: Global analyses of sea surface temperature, sea ice, and night marine air temperature since the late nineteenth century. *J. Geophys. Res.*, **108**, 4407, doi:10.1029/2002JD002670.

Smith, T. M., R. W. Reynolds, T. C. Peterson, and J. Lawrimore, 2008: Improvements to NOAA's historical merged land-ocean surface temperature analysis (1880-2006). *J. Clim.*, **21**, 2283–2296, doi:10.1175/2007JCLI2100.1.

Smoliak, B. V., J. M. Wallace, P. Lin, and Q. Fu, 2015: Dynamical Adjustment of the Northern Hemisphere Surface Air Temperature Field: Methodology and Application to Observations*. *J. Clim.*, **28**, 1613–1629, doi:10.1175/JCLI-D-14-00111.1.

Wu, Z., and N. E. Huang, 2009: Ensemble Empirical Mode Decomposition : A Noise Assisted Data Analysis Method. *Adv. Adapt. Data Anal.*, **1**, 1–41, doi:10.1142/S1793536909000047.